Journal Pre-proof

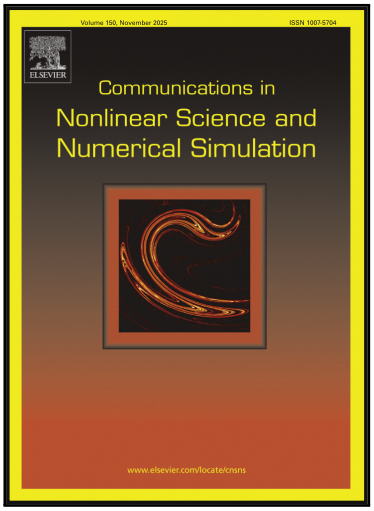

Tertiary, Quaternary and higher order states in the Sequence of Bifurcations Approach (SBA) to Turbulence for Laterally Heated Shear Flows within a Rectangular Tube

T. Akinaga, P. M J Trevelyan, S.C. Generalis

PII: S1007-5704(26)00117-6
DOI: https://doi.org/10.1016/j.cnsns.2026.109756
Reference: CNSNS 109756

To appear in: *Communications in Nonlinear Science and Numerical Simulation*

Received date: 26 September 2025
Revised date: 31 December 2025
Accepted date: 13 January 2026

Please cite this article as: T. Akinaga, P. M J Trevelyan, S.C. Generalis, Tertiary, Quaternary and higher order states in the Sequence of Bifurcations Approach (SBA) to Turbulence for Laterally Heated Shear Flows within a Rectangular Tube, *Communications in Nonlinear Science and Numerical Simulation* (2025), doi: https://doi.org/10.1016/j.cnsns.2026.109756

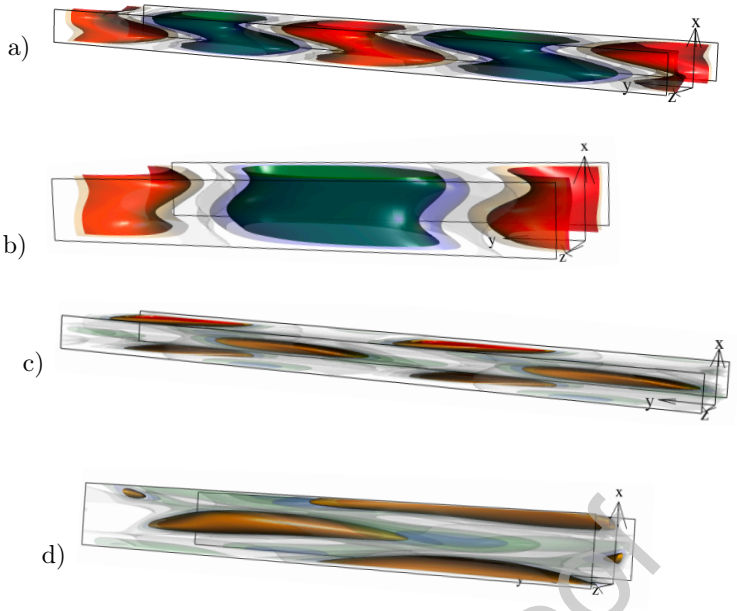

Graphical Abstract

Tertiary, Quaternary and higher order states in the Sequence of Bifurcations Approach (SBA) to Turbulence for Laterally Heated Shear Flows within a Rectangular Tube

T. Akinaga[a], P. M. J. Trevelyan[b], S. C. Generalis[b]

The tertiary OBV oscillatory states of the laterally heated rectangular tube in the SBA for $Pr = 0, Gr = 710$. The suharmonic state is a pulsating flow and it is depicted in a) for its azimuthal velocity and c) vorticity profiles. The equivalent superharmonic state is not pulsating and is depicted in b) for its azimuthal velocity and d) vorticity profiles. Here the wavenumbers are $(\alpha, \beta = 1.34, 0.7)$ for the subharmonic and $(\alpha, \beta = 1.34, 1.34)$ for the superharmonic state respectively.

Highlights

Tertiary, Quaternary and higher order states in the Sequence of Bifurcations Approach (SBA) to Turbulence for Laterally Heated Shear Flows within a Rectangular Tube

T. Akinaga[a], P. M. J. Trevelyan[b], S. C. Generalis[b]

- Research highlight 1 - Application of the fully deterministic Sequence of Bifurcations Approach
- Research highlight 2 - Vanishing flow through Lateral Section via imposition of a Constant Flux constraint
- Research highlight 3 - The remote ends of the rectangular tube are assumed to be closed/periodic
- Research highlight 4 - The large aspect ratio has potential to a variety of engineering applications

Tertiary, Quaternary and higher order states in the Sequence of Bifurcations Approach (SBA) to Turbulence for Laterally Heated Shear Flows within a Rectangular Tube

T. Akinaga[a], P. M. J. Trevelyan[b], S. C. Generalis[b*]

[a] *Faculty of Engineering Science, Akita University, 1-1 Tegata-Gakuen Machi, Akita, Akita-Shi 010-8502, Akita, Japan*
[b] *Aston Fluids Group, Aston University, , Birmingham, B4 7ET, United Kingdom*

Abstract

We consider a vertical rectangular tube of large aspect ratio with side-wall heating in order to mimic realistic experimental conditions. We therefore impose the condition that across any lateral cross-section of the rectangular tube the fluid flow vanishes. We find through our numerical analysis that oscillatory modes yield critical conditions and offer therefore sequential bifurcations that lead to the turbulent regime. Although the linear stability analysis is the same as the case where the imposed constant flux condition is absent, the corresponding nonlinear regime displays fundamentally different characteristics to the open narrow channel case. Here we focus on the sequence of bifurcations approach of a fluid enclosed in a rectangular tube, aligning with engineering applications. We additionally assume the limit of small Prandtl number and thus the effects caused by temperature perturbations are ignorable. Finally we identify the oscillatory states that lead to turbulence as the Grashof number increases up to the value 1000. Our fully nonlinear numerical analysis shows that all bifurcations are supercritical and here we concentrate on the critical axial wavenumber of the linear stability analysis of the laminar flow and its pairing with a specific azimuthal wavenumber.

Keywords: Incompressible flow, Bifurcation theory, nonlinearity, stability, turbulence, Floquet parameters, Convective flow
PACS: 76A05, 76Dxx, 70K30, 70K50

1. Introduction

Laterally heated flows without the imposition of a constant flux condition across any lateral section of the tube have received attention for many decades [1]-[2] due to the many applications in engineering, such as dwelling construction and cooling, ventilated double glazing (when combined with pressure flow), nuclear engineering, heat exchangers, aerodynamic surfaces, to mention a few. The pioneering works of Boyarintsev [1]-[3], Gershuni [4]-[5], Rudakov [6] Vest and Arpaci [7] and several others were concerned with the stability of natural convection between infinite vertical planes kept at different fixed temperatures. The case when thermal stratification is present in the vertical direction, was considered by Birikh et al. [8] and Korpela et al. [9] who determined that the instability was either shear or buoyancy driven, depending on the value of the Prandtl number Pr. It is interesting to note that the conductive state became unstable to stationary instabilities for $Pr < 12.7$ and oscillating thermal instabilities for $Pr > 12.7$. Their analysis was extended by Bergholz [10] to cover a larger range of stratification levels and Prandtl numbers revealing either traveling waves or standing waves are dominant, ie become critical before the steady solutions that appear first for lower stratification. The preferred pattern was studied independently by Fujimra and Mizushima [11], who accurately calculated the critical Prandtl number to be $Pr_c = 12.45425644$, and Kropp and Busse [12]. Both studies assumed weak nonlinearity and they studied a wide range of Prandtl numbers, concluding that for $Pr > Pr_c$, the dominant pattern is standing waves. Using weakly nonlinear analysis both studies further examined the nonlinear interaction spectrum between steady and oscillatory modes near the cross-over point and analysed the characteristics of the bifurcations at this bicritical point.

Stability in an annular enclosure of infinite length with the condition that the instability of the fluid flow is purely hydrodynamic (isothermal), and it is therefore applicable to a Boussinesq fluid with a small Prandtl number, for example the Prandl number for liquid metals, bounded between two infinite walls. This geometric set up was studied through the sequence of bifurcations approach in Nagata and Busse [13], hereafter referred to as NB. The only control parameter that governs the flow in this case is the Grashof number Gr as temperature decouples from the equations of motion. In their analysis NB obtained the bifurcation boundary of the secondary finite amplitude steady two-dimensional transverse roll vortices, as predicted by Squire's theorem [14]. NB proceeded to analyse numerically the stability characteristics of the secondary transverse vortices and they identified the Eckhaus [15] stability boundary and the bifurcation curve of steady as well as oscillatory three dimensional tertiary flow. During their analysis of the secondary solutions, NB identified

*Corresponding author. Electronic mail: s.c.generalis@aston.ac.uk

regions of the parameter space (α, Gr), where α is the wavenumber of the secondary transverse vortices, where nonlinear solutions could not be found numerically. The non-existence of nonlinear solutions was also encountered in Meyer-Spasche and Keller [16] and Paap and Riecke [17] in the Taylor vortex flow configuration. It has been analysed and explained subsequently to be due to the span of the linear stability curve in terms of the primary wavenumber α contributing to the $1:2$ spatial resonance. For a detailed explanation of this resonance see Fujimura and Mizushima [18] and Mizushima [19].

Ubiquitous flows, such as Couette flow, Plane Poiseuille flow, Taylor-Couette flow, Laterally Heated flow and their variants, because of their simple geometry and associated experiments, offer the perfect set up for our quest in identifying the inner mechanisms of turbulence through simulations thus paving the way in our understanding of how the fluid flow approaches this aperiodic regime as certain control parameters vary. For example, a new class of solutions, that provide a variant way to approach the turbulent regime previously unknown, were identified in plane Couette flow, which is known to be linearly stable for any value of the control parameter, the Reynolds number R. This was achieved by connecting two flows numerically for $Pr = 0$. For example, Itano and Generalis [20] obtained a vortical structure in isothermal plane Couette flow, having the shape of a hairpin vortex, via connecting Rayleigh—Bénard convection and plane Couette flow [21] through homotopy simulations. More recently the higher order bifurcation (stability) characteristics of the Taylor-Couette problem were studied numerically in [22] with good agreement established with the experimental results of [23].

The basic, or laminar, velocity profile of our flow includes an inflection point. Nagata and Busse [13], for the infinite long channel, found that the primary bifurcation is described by a steady two dimensional transverse vortex flow whereas the secondary bifurcation is characterised by steady three dimensional subharmonic sinusoidal motions of the transverse vortex. By identifying stability boundaries of increasing hierarchy in the deterministic sequence of bifurcations approach (SBA) to turbulence, engineers can predict and control flow instabilities in rotating machinery, chemical reactors, double glazing, heat storage and release, optimization of rotating equipment, such as turbines, centrifuges, mixers, cooling systems, electronic devices, and solar collectors, amongst other applications.

The present study explores the transition from laminar flow to turbulence in laterally heated shear flows within a closed rectangular tube of large aspect ratio, in order to identify the possibility of a new class of solutions by imposing the additional constraint of a vanishing fluid flux (this is apparent for the purely conductive state of Fig.1) across any lateral section of the tube. The equivalent case for identifying new classes of solutions for the purely rotating case was studied in [22]. It is thus identical to [13] at the purely conductive stage. After confirming the result of NB at the secondary bifurcation level, we show that as Gr is increased above its (second) critical value, a three dimensional periodic motion sets in as the tertiary flow. Observing that DNS (Direct Numerical Simulation) could capture several unstable periodic solutions representing a transient state, we find different types of motion coexist as stable or unstable solutions of the system at high Grashof numbers, i.e. well above the stability boundary of laminar flow. This finding strongly depends on our choice of the wavenumbers in the axial and azimuthal directions.

The basic equations and the geometric configuration of our problem are formulated and discussed in section 2. After formulating the problem in section 3 we expose the harmonic expansion that was employed in our analysis and the basic properties of the small gap approximation of an axially confined duct with an imposed constant flux condition. The problem here is equivalent to [22] where rotation is substituted by convection. In section 4 we survey the sequence of bifurcations of the transverse vortices with the critical wavelength and their subsequent bifurcations. The properties of solutions bifurcating from the two dimensional transverse vortices and from tertiary solutions depend rather strongly on the basic wavelength of the two dimensional vortices and are all supercritical. Hence in section 4 we describe the numerical methods applied for their solutions and outline stability routes for the higher order bifurcating states for the specific wavenumbers (α, β) of the azimuthal and axial directions that were chosen in identifying the bifurcation points of the higher order states in the (α, β, Gr) space. Our conclusions are given in section 5.

2. Mathematical formulation of the problem

We consider the incompressible fluid flow in the narrow gap between two vertical plates kept at uniform but different temperatures. The half gap width d between the two plates will be used as the length scale in the following and d^2/ν as the timescale, where ν is the kinematic viscosity of the fluid, see Fig.1. We introduce a Cartesian system of coordinates with the z-coordinate in the direction normal to the vertical walls, the x-coordinate in the azimuthal direction and the y-coordinate in the direction of the axis as shown in Fig. 1. The corresponding unit vectors will be denoted by $\boldsymbol{k}$, $\boldsymbol{i}$, $\boldsymbol{j}$. The dimensionless Navier-Stokes equations for the velocity $\boldsymbol{u}$ and temperature θ deviations from the purely conducive state can then be obtained in the form:

$$\left(\frac{\partial}{\partial t} + \boldsymbol{u}\cdot\nabla\right)\boldsymbol{u} = -\nabla\pi + \nabla^2\boldsymbol{u} - \frac{\boldsymbol{g}}{g}(Gr\ z + \theta), \tag{1}$$

$$\nabla\cdot\boldsymbol{u} = 0, \tag{2}$$

$$\frac{\partial\theta}{\partial t} + \boldsymbol{u}\cdot\boldsymbol{\nabla}\theta = Gr\ \boldsymbol{u}\cdot\boldsymbol{k} + \frac{1}{Pr}\nabla^2\theta. \tag{3}$$

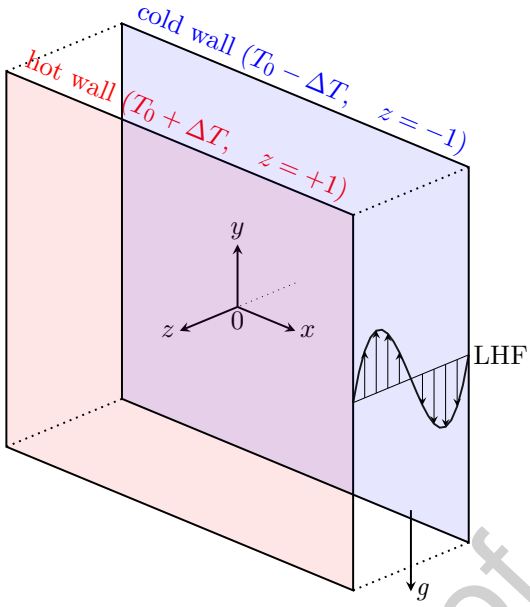

Figure 1: Laterally heated flow configuration. The dimensional gap width between the two finite plates is $2d$. The origin of the x, y and z coordinate reference system is positioned midplane and the side walls are kept at different temperatures. T_0 is the reference temperature.

where π is the pressure disturbance, Gr is the Grashof number defined by $Gr = \gamma g d^3 \Delta T/\nu^2$, $Pr = \dfrac{\nu}{\kappa}$, γ is the coefficient of thermal expansion, κ is the thermal diffusivity, ΔT is the temperature difference, and $g = |\boldsymbol{g}|$ is the acceleration due to gravity. The direction of gravity is given by $-\boldsymbol{j}$. The basic convective flow can be realised by taking a Boussinesq fluid between the vertical plates maintained at different constant temperatures, $T_0 + \Delta T$ and $T_0 - \Delta T$, see Fig.1, where T_0 is the ambient (reference) temperature. The conductive state is therefore represented by a linear temperature variation across the fluid layer, and buoyancy balances the viscous force. Since the basic laminar conductive flow profile violates the Rayleigh criteria [24] for the stability of shear flow profiles in the absence of viscosity, the bifurcation into a state of periodically arranged transverse vortices is supercritical for Prandtl number $Pr = 0$ as shown in NB. In this case the nondimensional laminar flow is given by the solution [4], [5]:

$$V_B(z) = Grz\left(1 - z^2\right)\boldsymbol{j}, \quad \theta = 0. \tag{4}$$

The boundary conditions for the velocity are given by

$$\boldsymbol{u} = \boldsymbol{0} \quad \text{at} \quad z = \pm 1, \tag{5}$$

In the present study, the Grashof number Gr plays a critical role in determining the flow's stability and bifurcation behaviour. As Gr increases, the flow transitions through various states, including steady two dimensional transverse vortex flow, oscillatory three dimensional subharmonic sinusoidal motions, and eventually three dimensional aperiodic motions at higher Gr values. These transitions highlight the importance of Gr in characterising the dynamics and stability of convective flows. In the limit of vanishing Prandtl number (heavy metals) temperature perturbations become identically zero and the energy equation decouples from the velocity equations. Further it is convenient to eliminate the equation of continuity by the introduction of the following general representation of the velocity field:

$$\boldsymbol{u} = U(t,z)\boldsymbol{i} + (V(t,z) + V_B(z))\boldsymbol{j} + \widetilde{\boldsymbol{u}}, \qquad \widetilde{\boldsymbol{u}} = \nabla \times (\nabla \times \boldsymbol{k}\phi) + \nabla \times \boldsymbol{k}\psi. \tag{6}$$

By using the operators $\boldsymbol{k} \cdot \nabla \times (\nabla \times\ )$, and $\boldsymbol{k} \cdot \nabla \times$ on Eq.(1) we obtain the following two equations for ϕ, the poloidal part, and ψ the toroidal parts of the velocity field of Eq.(6):

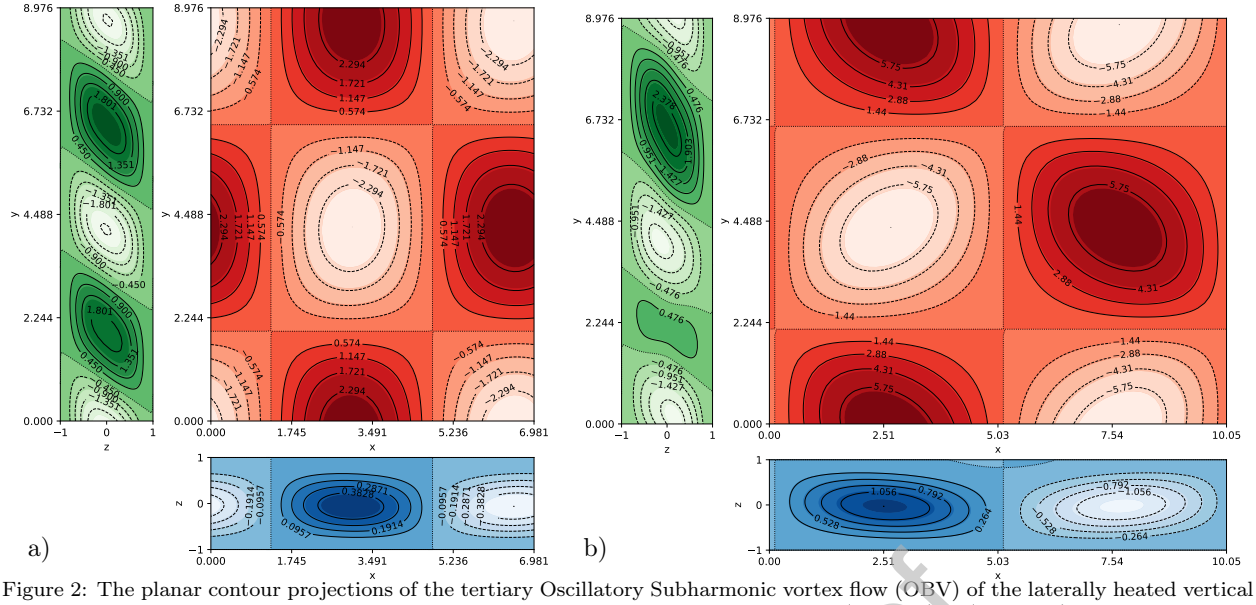

Figure 2: The planar contour projections of the tertiary Oscillatory Subharmonic vortex flow (OBV) of the laterally heated vertical rectangular tube realised in the configuration of Figure 1. The results of the present analysis with $(L, M, N) = (21, 10, 10)$ are given for the two values of the Grashof number in the SBA, for $Pr = 0$: (a) $Gr = 515$ and (b) $Gr = 540$ and $(\alpha, \beta) = (1.34, 0.7)$.

$$\left(\nabla^2 - \frac{\partial}{\partial t}\right)\nabla^2\triangle_2\phi = U\frac{\partial}{\partial x}\nabla^2\triangle_2\phi - \frac{\partial^2 U}{\partial z^2}\frac{\partial}{\partial x}\triangle_2\phi$$
$$-\frac{\partial^2 V}{\partial z^2}\frac{\partial}{\partial y}\triangle_2\phi + V\frac{\partial}{\partial y}\nabla^2\triangle_2\phi + \boldsymbol{k}\cdot\nabla\times\left(\nabla\times(\widetilde{\boldsymbol{u}}\cdot\nabla\widetilde{\boldsymbol{u}})\right), \tag{7}$$
$$\left(\nabla^2 - \frac{\partial}{\partial t}\right)\triangle_2\psi = U\frac{\partial}{\partial x}\triangle_2\psi - \frac{\partial U}{\partial z}\frac{\partial}{\partial y}\triangle_2\phi$$
$$+V\frac{\partial}{\partial y}\triangle_2\psi + \frac{\partial V}{\partial z}\frac{\partial}{\partial x}\triangle_2\phi - \boldsymbol{k}\cdot\nabla\times(\widetilde{\boldsymbol{u}}\cdot\nabla\widetilde{\boldsymbol{u}}), \tag{8}$$

and the following two equations for the mean flows in the azimuthal and axial directions, respectively:

$$\left(\frac{\partial^2}{\partial z^2} - \frac{\partial}{\partial t}\right)U = -\frac{\partial}{\partial z}\overline{\triangle_2\phi\left(\frac{\partial^2}{\partial x\partial z}\phi + \frac{\partial}{\partial y}\psi\right)}, \tag{9}$$
$$\left(\frac{\partial^2}{\partial z^2} - \frac{\partial}{\partial t}\right)V = -\frac{\partial}{\partial z}\overline{\triangle_2\phi\left(\frac{\partial^2}{\partial y\partial z}\phi - \frac{\partial}{\partial x}\psi\right)}. \tag{10}$$

In the arrangement that is explored in the present study ($Pr = 0$), only eqs.(7-10) in conjunction with eq.(4) will be retained. We note that the time dependence of the mean components of eqs.(9-10) has been neglected, since we are interested in flow states that exist under steady external conditions. We note here that U, V are the mean flows in the azimuthal (x) and axial (y) directions, respectively. Note that the mean flow V (for the axial direction), was not considered in [13], in contrast to the present study, where the mean flows in both directions are being considered. We note that the overbar indicates the average over the $x-$ and $y-$coordinates and the operator $\triangle_2$ is defined by $\triangle_2 \equiv \nabla^2 - (\boldsymbol{k}\cdot\nabla)^2$. The case where the system was under axial rotation and $Gr = 0$ was studied in [22], while in the present study we concentrate on the case where rotation is absent and $Gr \neq 0$. The case where a parabolic transverse seepage was applied with in the absence of axial rotation $Gr \neq 0$ was considered in [25].

3. Harmonic expansion

In order to implement the deterministic approach of the sequence of bifurcations for higher order states that emanate from disturbing the laminar flow of eq.(4) we assume periodicity in stream-wise (x) and span-wise (y) directions, whereas the non-slip boundary conditions at the boundaries in the wall coordinate are assumed. The linear stability boundary is given in [13] and is adopted in the present analysis. In order to follow the bifurcating higher order states for the poloidal

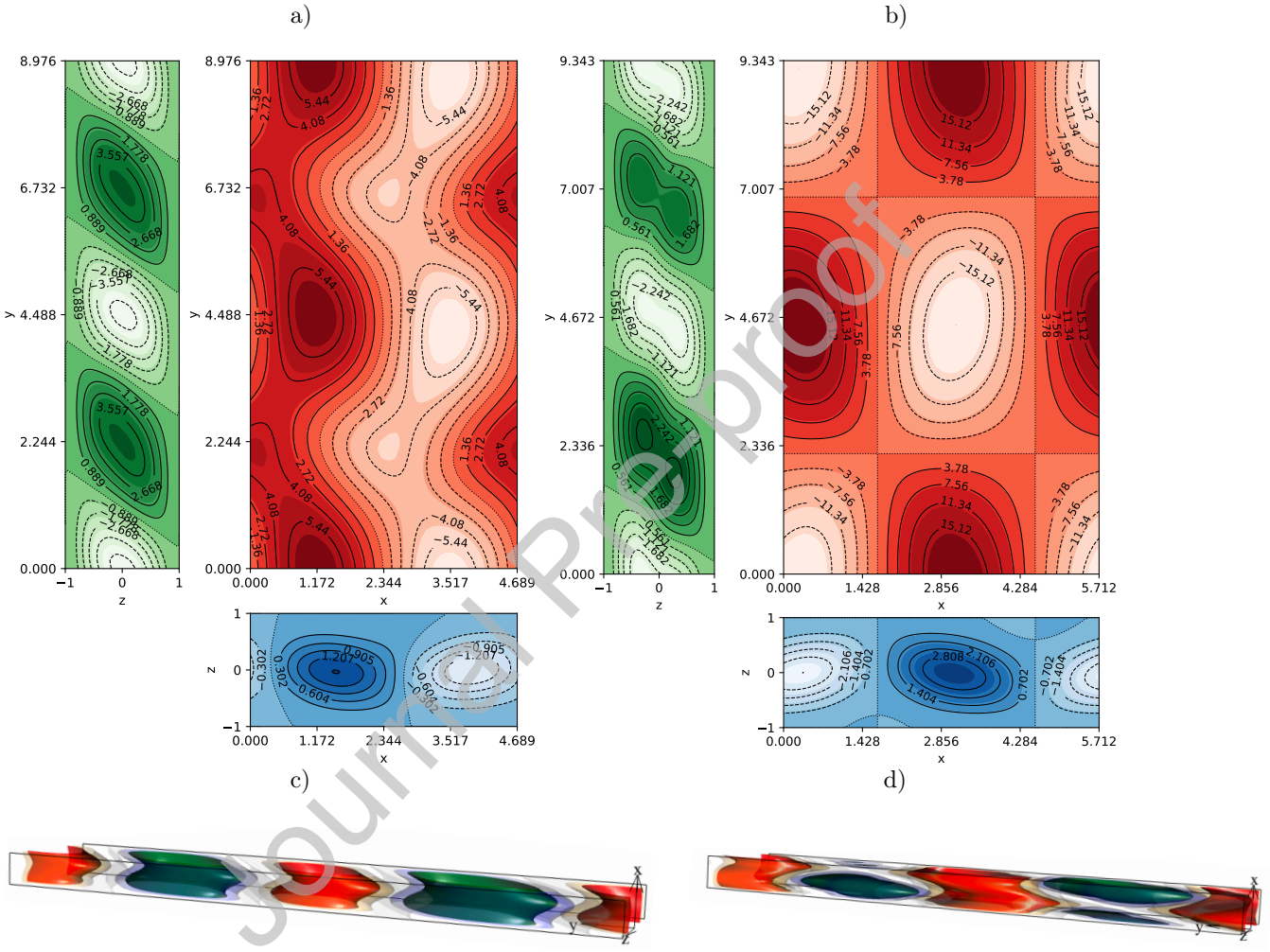

Figure 3: The quaternary Oscillatory Subharmonic Azimuthally Drifting (OSAD) vortex flow and the tertiary state OBV of the laterally heated vertical rectangular tube of Figure 1. The results of the present analysis with $(L, M, N) = (21, 10, 10)$ are given, for $Pr = 0$. Here for $Gr = 593$ ((a,c) left column) and $Gr = 640$ ((b,d) right column) the quaternary OSAD and the tertiary OBV states respectively. The states are depicted by the three planar countour plots (top - as shown) and by the azimuthal $\boldsymbol{u}$ profile, bottom figures. Here $(\alpha, \beta) = (1.34, 0.7)$.

(ϕ) and toroidal (ψ) parts in equation (6), we performed a normal mode analysis assuming the following expansions

$$\phi\left(x,y,z\right)=\sum_{\ell=0}^{L}F_{\ell}(z)\widehat{\phi}_{\ell}, \tag{11}$$

$$\psi\left(x,y,z\right)=\sum_{\ell=0}^{L}G_{\ell}(z)\widehat{\psi}_{\ell}, \tag{12}$$

where:

$$\widehat{\phi}_{\ell}=\sum_{(m,n)\neq(0,0)}^{|m|\leq M,|n|\leq N}a_{\ell mn}\,e^{i[m\alpha(x-c_{x}t)+n\beta(y-c_{y}t)]}, \tag{13}$$

$$\widehat{\psi}_{\ell}=\sum_{(m,n)\neq(0,0)}^{|m|\leq M,|n|\leq N}b_{\ell mn}\,e^{i[m\alpha(x-c_{x}t)+n\beta(y-c_{y}t)]}, \tag{14}$$

where in the above expressions α,β are the wavenumbers in the azimuthal and axial directions respectively, $a_{\ell mn},b_{\ell mn}$ are the unknown complex coefficients to be determined and where we have additionally introduced c_x,c_y, the constant phase speeds in the azimuthal an axial directions, in order to also take into account shape preserving traveling wave solutions in the azimuthal and/or axial directions. The phase speed c can be determined via a geometric method or can be evaluated independently. In our studies we use a Galerkin-type approach that is capable of following the solution if it moves with a phase speed c. In this case the phase speed is one of the unknown parameters and can also be determined explicitly by our numerical method as one of the unknown parameters. Care therefore has to be exercised in positioning the phase speed within the matrix of the unknown coefficients. In our analysis, however, and with the exception of the two dimensional solution, we only identified solutions of the form

$$\widehat{\phi}_{\ell}=\sum_{(m,n)\neq(0,0)}^{|m|\leq M,|n|\leq N}a_{\ell mn}(t)\,e^{i[m\alpha(x-c_{x}(t)t)+n\beta(y-c_{y}(t)t)]}, \tag{15}$$

$$\widehat{\psi}_{\ell}=\sum_{(m,n)\neq(0,0)}^{|m|\leq M,|n|\leq N}b_{\ell mn}(t)\,e^{i[m\alpha(x-c_{x}(t)t)+n\beta(y-c_{y}(t)t)]}, \tag{16}$$

i.e. solutions where the complex coefficients $a_{\ell mn}(t),b_{\ell mn}(t)$ are time dependent, while simultaneously there exist time dependent (not constant as in eqs. (13-(14)) $\boldsymbol{c}(t)=(c_x(t),c_y(t))\neq 0$ indicating solutions that are drifting in either the axial, or azimuthal or both directions with variable phase speeds. As a measure of nonlinearity we choose the time dependent poloidal and toroidal norms $\ell_2^{\phi}(t),\ell_2^{\psi}(t)$, respectively, defined by

$$\ell_2^{\phi}(t)=\sqrt{a_{\ell mn}(t)a^{*}_{\ell mn}(t)},\ \ell_2^{\psi}(t)=\sqrt{b_{\ell mn}(t)b^{*}_{\ell mn}(t)}, \tag{17}$$

of the nonlinear solution states that we identified. Here the * indicates the complex conjugate. The following equations were used for the mean flows in the azimuthal and axial directions

$$U\left(z\right)=\sum_{\ell=0}^{L}G_{\ell}(z)\;c_{\ell}(t), \tag{18}$$

$$V\left(z\right)=\sum_{\ell=0}^{L}G_{\ell}(z)\;d_{\ell}(t)+\mu\;(z^{2}-1), \tag{19}$$

where the parameter μ is determined by the condition of vanishing mass flux in the y-direction,

$$\int_{-1}^{+1}V(z)\,dz=0 \tag{20}$$

and $c_\ell(t),d_\ell(t)$ are the mean flow coefficients in the azimuthal and axial directions, respectively and Eq. (19), the constant flux condition of a vanishing flow rate through any lateral cross-section, ensures that the remote ends of the of the rectangular tube in the axial direction are assumed to be closed and that our numerical model is thus a better reflection of the real life experimental set-ups. A variant of the above methodology was used to identify the states for the rotating case, the Taylor-Couette problem, and when convective effects are removed, with good agreement between simulations

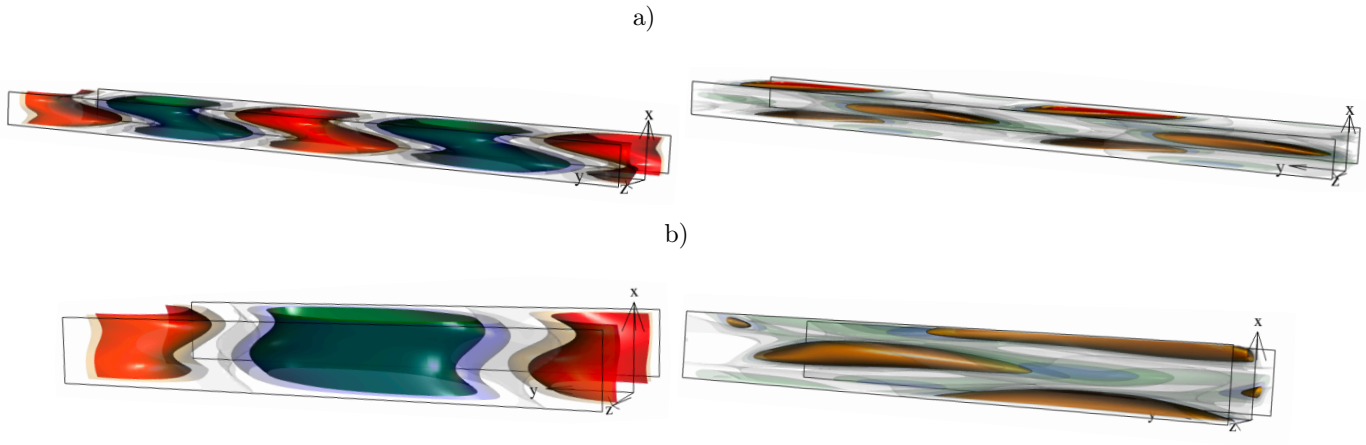

Figure 4: The tertiary OBV and OPV oscillatory states of the laterally heated rectangular tube. The results of the present analysis with $(L, M, N) = (21, 10, 10)$ are given, for $Pr = 0, Gr = 710$. The state is a pulsating flow and it is depicted at ((a) – left) for its azimuthal velocity and ((a) - right) vorticity profiles. The equivalent superharmonic state is not pulsating and is depicted in ((b) – left) for its azimuthal velocity and ((b) - right) vorticity profiles. A total of 4×10^9 time steps were required to produce the figures depicted here. Here $(\alpha, \beta = 1.34, 0.7)$ for the subharmonic OBV and $(\alpha, \beta = 1.34, 1.34)$ for the superharmonic OPV states respectively.

[22] and experiment [23] and also for the comparisons between the results of [22] and the numerical analysis of [26], where eq.(10) was not employed.

The $F_\ell(z)$ and $G_\ell(z)$ $(\ell = 0, 1, \ldots, L)$ of eqs.(11-12) are combinations of the 1st kind Chebyshev polynomials ($T_\ell(z)$ $(\ell = 0, 1, \ldots)$),

$$F_\ell(z) = \frac{(\ell+1)\,T_{\ell+4}(z) - 2\,(\ell+2)\,T_{\ell+2}(z) + (\ell+3)\,T_\ell(z)}{4\,(\ell+2)}, \tag{21}$$

$$G_\ell(z) = \frac{T_\ell(z) - T_{\ell+2}(z)}{2}, \tag{22}$$

that are employed in order to satisfy

$$F_\ell(z = \pm 1) = 0, \tag{23}$$

$$\frac{dF_\ell}{dz}(z = \pm 1) = 0, \tag{24}$$

$$G_\ell(z = \pm 1) = 0. \tag{25}$$

As an example of the poloidal toroidal decomposition above we can write for $\widetilde{\boldsymbol{u}}$ of equation (6)

$$\widetilde{\boldsymbol{u}} = \left(\frac{\partial^2 \phi}{\partial x \partial z} + \frac{\partial \psi}{\partial y}\right)\boldsymbol{i} + \left(\frac{\partial^2 \phi}{\partial y \partial z} - \frac{\partial \psi}{\partial x}\right)\boldsymbol{j} - (\triangle_2 \phi)\,\boldsymbol{k}. \tag{26}$$

The integer values L, M, N, the predetermined truncation levels, have to be sufficiently high such that the nonlinear solutions, measured by $\ell_2^\phi(t), \ell_2^\psi(t)$ of eqs.(17), do not change significantly if L, M, N are increased, and a change $\leq 1\%$ is achieved. In our studies a typical set of truncation levels for the reported tertiary, quaternary and quinary states with $L = 17, M = 10, N = 10$ were in general sufficient in order to account for the subharmonic instability $2:1$ [13]. The subharmonic instability is the instability whereby the dominant higher order state has a wavenumber that equals half the wavenumber of the lower order state in the bifurcation tree of the sequential bifurcations as the Gr number value increases. For the verification of our results and for the subharmonic instability in particular the truncation levels with $L = 21, M = 12, N = 12$ were also selected. This inevitably results in a large number of complex coefficients $a_{\ell mn}(t), b_{\ell mn}(t), c_\ell(t)$ and $d_\ell(t)$ from Eqs.(7-10), that need to be determined. We can reduce the number of coefficients to be calculated by using relationships such as,

$$a_{\ell -m -n}(t) = a^*_{\ell mn}(t), \tag{27}$$

because of the reality conditions of the coefficients, resulting from $\phi = \phi^*$ and $\psi = \psi^*$, where ϕ^*, ψ^* refer to the complex conjugate of ϕ, ψ, respectively. Additional relations that refer to the symmetries of the higher order nonlinear states that are sought are also used, see Table 1. This reduces the number of coefficients further and makes the study of the nonlinear solutions, at relatively high truncation levels, possible with the additional benefit of reduced computation time.

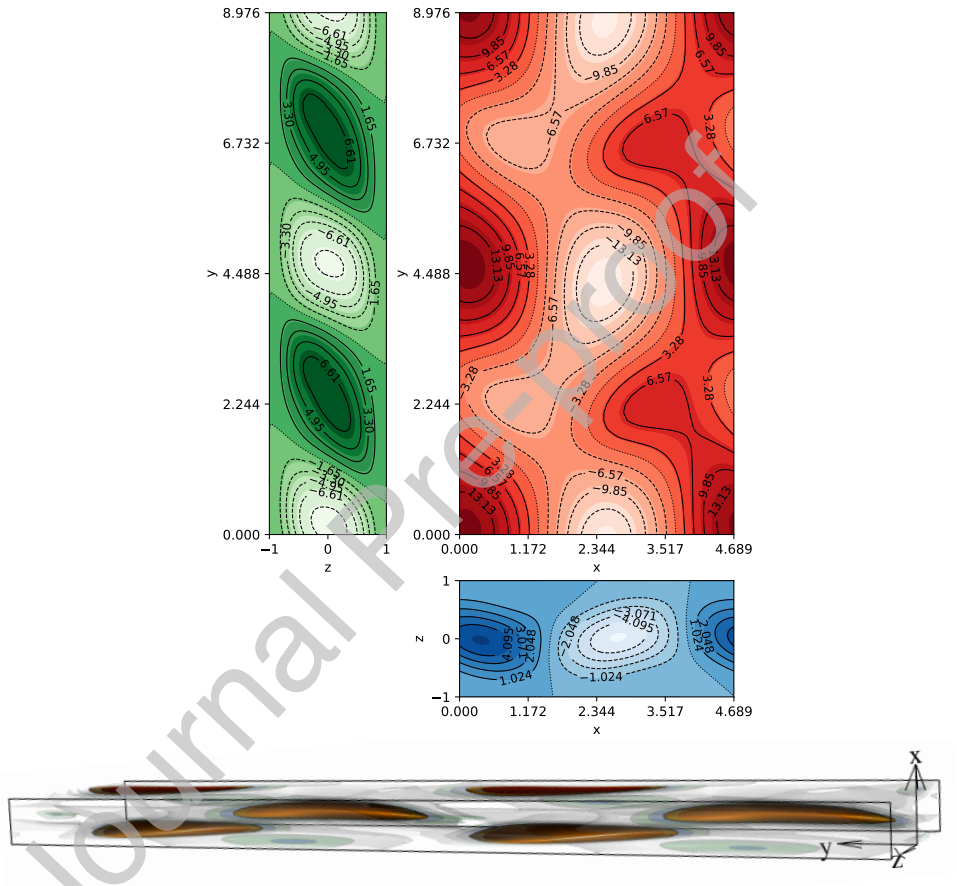

Figure 5: The planar contour projections of the Oscillatory Subharmonic Quinary axially and azimuthally drifting state (OSAZD) of the laterally heated rectangular tube top set and its vorticity field profile bottom figure. The results of the present analysis with $(L, M, N) = (21, 10, 10)$ are given, for $Pr = 0, Gr = 770$. A total of 2×10^9 time steps were required to produce the figures depicted here. Here $(\alpha, \beta) = (1.34, 0.7)$. The state bifurcates from the quaternary state with $(\alpha, \beta) = (1.34, 0.7)$ and has the same wavenumbers.

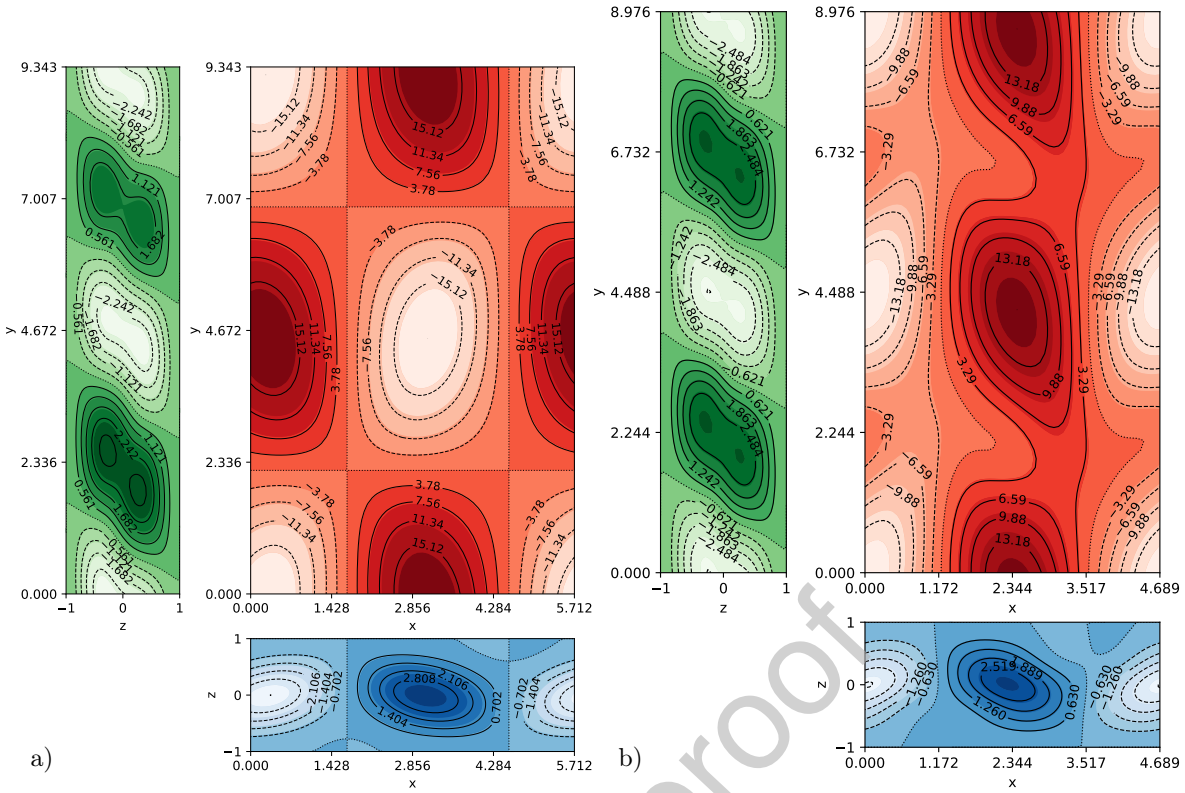

Figure 6: Planar contour projections of the tertiary subharmonic states OBV at different values of Gr. The results of the present analysis with $(L, M, N) = (21, 10, 10)$ are given, for $Pr = 0, Gr = 640(a), 740(b)$ are presented here. For both states $(\alpha, \beta) = (1.34, 0.7)$. The states were captured via DNS. A higher truncation level with $(L, M, N) = (23, 14, 14)$ was also applied to ensure that the states were captured accurately.

Direct Numerical Simulations (DNS) were employed for all the cases since time dependent solutions needed to be determined and these solutions do not lead to steady states or shape preserving traveling waves. The evolution in time of the oscillatory states is analysed through second order integration in time of the system of equations for the expansion coefficients $\phi_{\ell mn}(t)$ and $\psi_{\ell mn}(t)$ in the general representation (13-14). The truncation level is determined in the same way as in the case of steady state solutions or shape preserving traveling waves, see [22]. In order to determine the stability range of these oscillatory states we introduce perturbations on the leading coefficients and observe their evolution in time. Any oscillatory state is considered stable for the range of Grashof numbers, for which a converged solution (that remains unchanged with further time integrations or increased truncation levels) can be identified.

4. SBA - The search for higher order sates

All our efforts are directed towards an improved understanding of turbulent fluid flow and are based on the fully deterministic sequence of bifurcations approach (SBA). It is therefore the aim of this manuscript to demonstrate that using Eqs.(7-10) solutions of the isothermal Navier-Stokes equations of motion can help us understand the underlying dynamical mechanisms operating in turbulent fluid systems and additionally make a stronger connection between theory/simulation and experiment whenever laboratory results are available. The SBA allows us to follow the spatially and temporally periodic solutions of the Navier-Stokes equations prior to the exhibition of their chaotic nature allowing us to analyse the patterns that are formed when turbulence is evident for the particular system under consideration. By analysing the formation of these turbulent patterns, we can study the transport mechanism that operates under turbulent conditions at the values of the control parameter, that for the present study is the Grashof number, measuring the strength of the applied heating. It is through this route that we can identify the fundamental frequencies upon the combination of which the aperiodic motion is built.

We provide here a brief description of the different numerical schemes that we employed in the present study and frequently employ in general in our studies for the transition to turbulence through the SBA approach. The Newton-Raphson method is used for steady, time independent, and travelling-wave type equilibrium states with uniform phase speed, see eqs.(13-14). Substitution of the expansions of eqs.(11-14) with the appropriate truncation level L, M, N into the equations (7-8) leads to to a set of nonlinear algebraic equations for the expansion coefficients, $a_{\ell mn}, b_{\ell mn}$, c_ℓ, d_ℓ, which when combined with the Chebyshev-Gauss-Lobatto collocation method yield the solutions for $a_{\ell mn}, b_{\ell mn}$, c_ℓ, d_ℓ, c_x, c_y. In order to investigate the stability characteristics of the steady or periodic solutions (travelling-wave type equilibrium states that drift with a constant phase speed $\mathbf{c} = (c_x, c_y)$) we use linear stability analysis on the established time independent

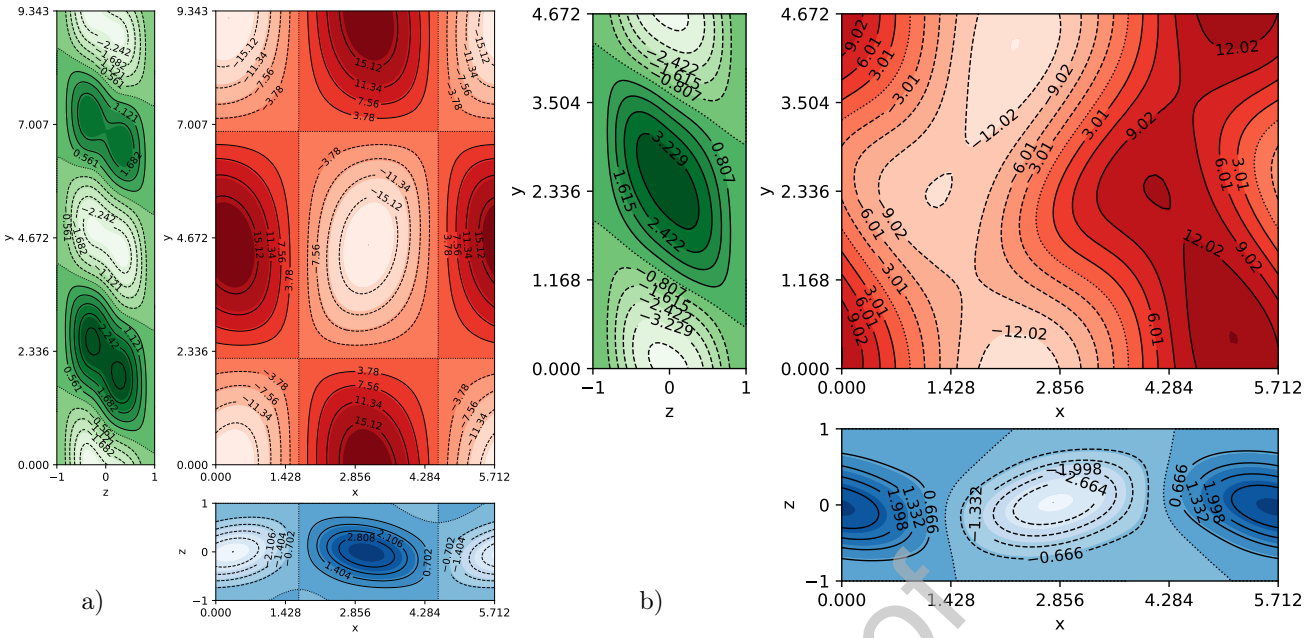

Figure 7: The quaternary OSAD (drifting in the azimuthal direction) subharmonic state and the tertiary Oscillatory Superharmonic axially drifting (OPV) flow of the laterally heated vertical rectangular tube of Figure 1: (a) the quaternary OSAD and right column (part b) the tertiary OPV and for $Gr = 640$. The results of the present analysis with $(L, M, N) = (21, 10, 10)$ are given, for $Pr = 0$. The states are depicted by their planar countour plots. Here $(\alpha, \beta) = (1.34, 1.34)$ for OPV and $(\alpha, \beta) = (1.34, 0.7)$ for OSAD. Both states were captured via DNS.

nonlinear solutions of section 3 . We superimpose three dimensional infinitesimal disturbances on these nonlinear solutions using Floquet theory and analyse the resulting eigenvalue spectrum. This procedure was followed for the secondary state only, as this was the only state that could be described with time independent coefficients in our study.

Accordingly if we let the generic infinitesimal disturbances to be of the form

$$\widetilde{\phi}_\ell = \sum_{\ell=0}^{L} F_\ell(z) \sum_{(m,n)\neq(0,0)}^{|m|\leq M,|n|\leq N} \widetilde{a}_{\ell mn}\, e^{i[(m\alpha+d)(x-c_x t)+(n\beta+b)(y-c_y t)]+\sigma t}, \tag{28}$$

$$\widetilde{\psi}_\ell = \sum_{\ell=0}^{L} G_\ell(z) \sum_{(m,n)\neq(0,0)}^{|m|\leq M,|n|\leq N} \widetilde{b}_{\ell mn}\, e^{i[(m\alpha+d)(x-c_x t)+(n\beta+b)(y-c_y t)]+\sigma t}, \tag{29}$$

we see that the coefficients are time independent and that the above two parameter (d, b) Floquet ansatz applies for a general type of three-dimensional disturbances since our solutions are assumed periodic in the azimuthal and axial dimensions (large aspect ratio of the rectangular tube) and include the cases where nonlinear solutions are of the travelling wave form (if they are steady ($c = 0$)), since in our calculations we employ a moving frame analysis to capture these states. Since we assumed that the value of $d^2 + b^2 \neq 0$ in the stability analysis no disturbances to eqs.(9-10) need to be taken into account into the stability analysis, thus reducing slightly the computational time required to calculate the eigenvalue spectrum. Equations (28) and (29) give rise to a linear homogeneous system for the unknowns $\widetilde{a}_{\ell mn}, \widetilde{b}_{\ell mn}$ with the growth rate σ providing the set of eigenvalues. The eigenvalue matrix, being approximately 30% larger than the matrix that identifies the steady nonlinear/travelling-wave type equilibrium solution, necessitates the use of high performance computing power to maintain the same accuracy for the eigenvalue spectrum as for the identified nonlinear solutions.

In the present study however, the nonlinear states, that are realised when the lowest within SBA hierarchically state is perturbed (the two dimensional state), have time dependent coefficients presented in eqs.(15-16), and Floquet analysis is not appropriate for these higher order states. The time development of the disturbance in this case followed in space and time by a direct numerical simulation (DNS). This is achieved by performing the time integration on the wall-normal components, w for the velocity and ω_z for the vorticity, derived from the full Navier-Stokes equations by using direct imposition of additional factors (boundary conditions), so that the the poloidal and toroidal parts satisfy the boundary conditions automatically, see eqs.(11-14, 18-19), while the Fourier expansions are employed in the streamwise and spanwise directions with the Chebyshev polynomial expansion employed in the direction normal to the plates. In our present study we employed the Newton-Raphson method to identify the only steady nonlinear state, namely the two dimensional secondary state. All higher order states in the SBA to the turbulent regime were calculated via time step forwarding through DNS.

Orders	States	Symmetry	Subharmonic route	Superharmonic route
Secondary	2d Vortex	Translation in time, reflection $a_{\ell-m} = a_{\ell m}$, shift (translation) in roll axis $\phi(y + 2\pi/\alpha, z) = \phi(y, z)$	VF	VF
Tertiary	Oscillatory	$a_{\ell-mn} = -a_{\ell mn}, m + n =$ even, $\ell =$ odd/even ($\ell =$ odd/even, $c_\ell = 0$), ($\ell =$ odd, $d_\ell \neq 0$)	OBV flow (Oscillatory Subharmonic Vortex) flow	
Tertiary	Oscillatory and axially drifting	$a_{\ell-mn} = -a_{\ell mn}, m + n =$ /odd ($\ell =$ odd, $c_\ell \neq 0$), ($\ell =$ even, $d_\ell \neq 0$)		OPV flow (Oscillatory Superharmonic Vortex)
Quaternary	Oscillatory and axially drifting	$a_{\ell-mn} = (-1)^\ell a_{\ell mn}, m + n =$ even/odd ($\ell =$ odd, $c_\ell \neq 0$, $\ell =$ even, $d_\ell \neq 0$)	OSAD flow (Oscillatory Subharmonic axially (u-drift) flow)	—
Quinary	Oscillatory axially and azimuthally drifting	$a_{\ell-mn} = (-1)^\ell a_{\ell mn}, m + n =$ even/odd ($\ell =$ even, $c_\ell \neq 0$), ($\ell =$ even, $d_\ell \neq 0$) ($\ell =$ odd, $c_\ell \neq 0$), ($\ell =$ odd, $d_\ell \neq 0$)	OSAZD flow (Oscillatory Subharmonic axially and azimuthally (u-drift and v-drift) flow)	—

Table 1: Nomenclature for states of flow and their symmetries in the present study. Note that the superharmonic and the subharmonic tertiary states share the same acronym.

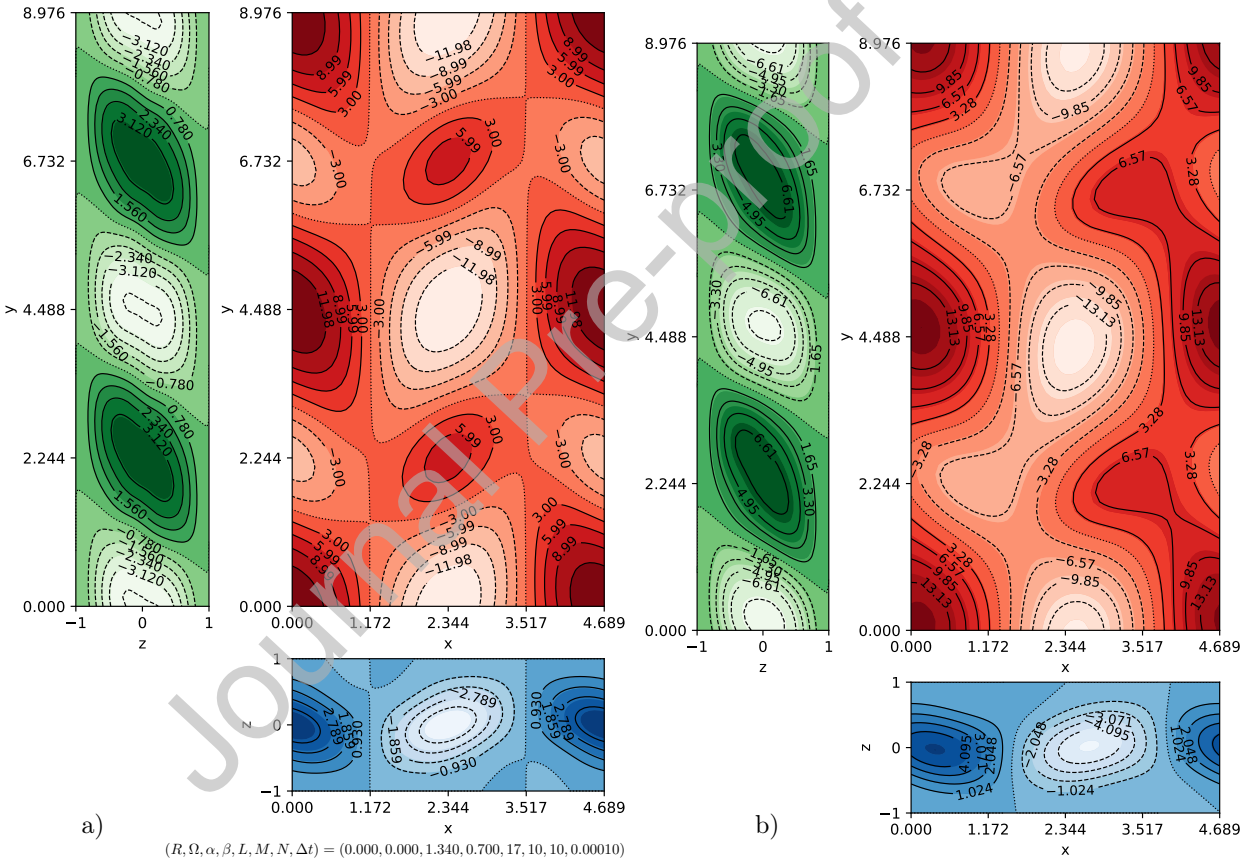

Figure 8: Comparison between the subharmonic tertiary OBV (a) and the quinary azimuthally and the suharmonic axially drifting state (OSAZD) of the laterally heated rectangular tube. The results of the present analysis with $(L, M, N) = (23, 14, 14)$ are depicted for $Pr = 0$ and $Gr = 710$ (left) and $Gr = 770$ (right). The quinary state bifurcates from the quaternary state of Fig.7 at $Gr = 770$ and has the same wavenumbers $(\alpha, \beta) = (1.34, 0.7)$ as the tertiary OBV.

SBA - results for the subharmonic $\alpha = \beta/2$ and superharmonic $\alpha = \beta$ cases

The first case involves tertiary states that bifurcate supercritically from the secondary states of NB . Additionally, we note that we can write for $\widetilde{\boldsymbol{u}}$ in (6):

$$\widetilde{\boldsymbol{u}} = \widetilde{u}\boldsymbol{i} + \widetilde{v}\boldsymbol{j} + \widetilde{w}\boldsymbol{k} = \nabla \times \boldsymbol{i}\phi_1 + \nabla \times \boldsymbol{j}\phi_2 + \nabla \times \boldsymbol{k}\psi, \tag{30}$$

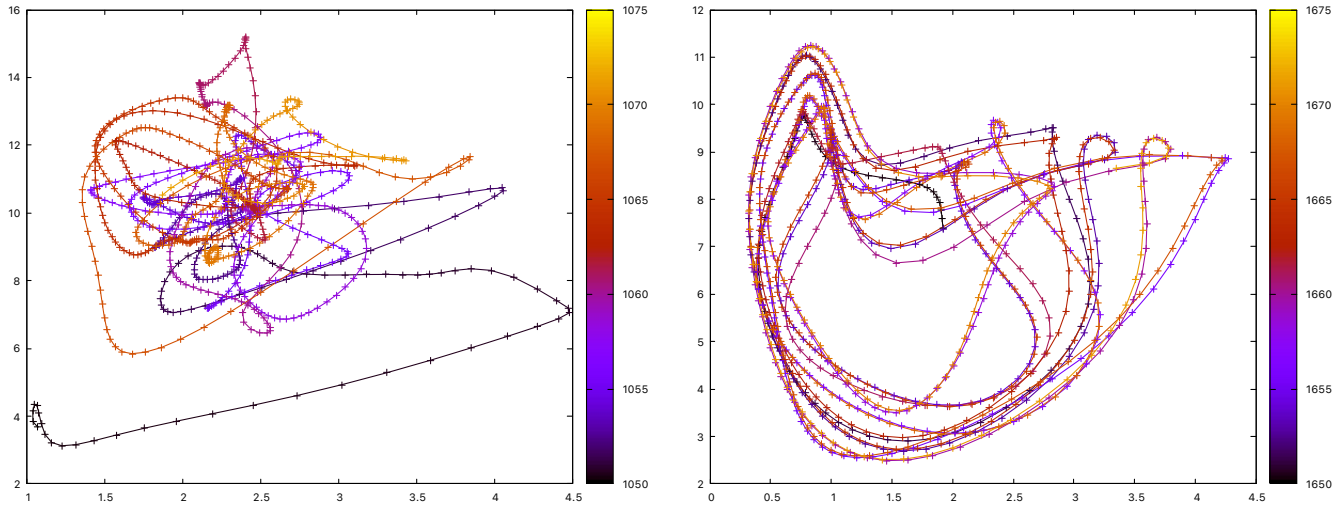

Figure 9: Transition to turbulence for the the Quinary oscillatory subharmonic state (left) and the Oscillatory tertiary superharmonic state (right). Both states are drifting in both axial and azimuthal directions of the laterally heated rectangular tube. The results of the present analysis are given, for $Pr = 0, Gr = 1000$ for both cases are presented. A total of 2×10^{10} time steps were required to produce the figures depicted here. Here $(\alpha, \beta) = (1.34, 0.7)$ for the subharmonic state on the left and $(\alpha, \beta) = (1.34, 1.34)$ for the superharmonic state on the right. The $\ell_2^{\phi}(t)$ norm (left ordinate) and $\ell_2^{\psi}(t)$ norm (right ordinate) of eqs.(17) are depicted here.

where

$$\phi_1 = \frac{\partial \phi}{\partial y}, \quad \phi_2 = -\frac{\partial \phi}{\partial x}. \tag{31}$$

Formulae (30, 31) allow us to present a three-dimensional graphic representation of the velocity field, through contour plots of the potentials ψ, ϕ_1, ϕ_2 in the planes perpendicular to $\boldsymbol{i}$, $\boldsymbol{j}$, or $\boldsymbol{k}$, which is exploited in the following.

The SBA analysis for this work produced the following results for the subharmonic route. As is known from [13], the secondary vortex flow (VF) bifurcates at $Gr = 497$ and is a steady two dimensional vortex. We confirm this finding and find that the two dimensional axial vortex bifurcates around $Gr = 500$. In order to study the stability of the two dimensional axial vortex there are two routes [13] to higher order nonlinear states in the SBA to turbulence, namely the subharmonic route and the superharmonic route. For the subharmonic route we choose $(\alpha, \beta) = (1.34, 0.7)$ and for the superharmonic route we choose $(\alpha, \beta) = (1.34, 1.34)$ for our present study.

The tertiary Oscillatory Subharmonic vortex (OBV) flow with $(\alpha, \beta) = (1.34, 0.7)$ appears at $Gr = 515$ and the coefficients observe the conditions $m+n$ =even for $a_{\ell mn}$ and $m+n$ =odd for $b_{\ell mn}$ for ℓ even or odd. This state is depicted in Figure 2. The planar contour projections of the tertiary OBV of the laterally heated vertical rectangular tube are given for the two values of the Grashof number in the SBA, for $Pr = 0$. For part (a) of the Figure 2 $Gr = 515$ and for part (b) $Gr = 540$. Here $(\alpha, \beta) = (1.34, 0.7)$. The state bifurcates from the secondary transverse vortex with $\alpha = 1.345$ of [13]. The truncation levels required for the DNS calculations to capture the oscillatory state are such that the tolerance criteria are indicated in Figure 2. We see in Figure 2 that as Gr away from the bifurcation point of the tertiary flow the orientation of the vortices becomes increasingly skewed to maximase mass transport.

Maintaining the same wavenumber values $(\alpha, \beta) = (1.34, 0.7)$ and increasing the value of Gr we encounter the quaternary Oscillatory Subharmonic Azimuthally Drifting (OSAD) vortex flow of the laterally heated vertical rectangular tube in Figure 3. The results of the present analysis with $(L, M, N) = (21, 10, 10)$ are given, for $Pr = 0$. Here for $(a, c), Gr = 593$ (left column) and $(b, d), Gr = 640$ (right column). The states are depicted in Figure 3 by their planar countour plots (top - (a,b)) and by their vorticity (bottom - (c,d)) countour profile. The OSAD required a total of 3×10^9 forward time steps at this higher truncation level to produce the figures depicted here. The state bifurcates from the tertiary state OBV of Figure 2 and has the same wavenumbers $(\alpha, \beta) = (1.34, 0.7)$). This state cannot be identified by the Newton Raphson method as it is not a steady localised or a uniformly drifting wave solution. We identified three stable regions of the quaternary flow: $593 \leq Gr < 640$, $649 \leq Gr \leq 660$ and $740 \leq Gr < 770$, see Table 2. The subharmonic state returns to its tertiary status in between these regions and for $G \geq 770$ we have the formation of the quinary subharmonic state.

In Figure 4 we depict the tertiary pulsating OPV state of the laterally heated rectangular tube with pulsating nature. The results of the present analysis with $(L, M, N) = (21, 10, 10)$ are given, for $Pr = 0, Gr = 710$. The state is a pulsating flow and it is depicted at ((a) – left) for its axial velocity and ((a) - right) vorticity profiles. The equivalent superharmonic state is depicted in ((b) – left) for its axial velocity and ((b) - right) vorticity profiles. A total of 4×10^9 time steps were required to produce the figures depicted here. Here $(\alpha, \beta) = (1.34, 0.7)$ for OSAD and $(\alpha, \beta) = (1.34, 1.34)$ for

Orders	States	Gr Range	Subharmonic route	Superharmonic route
Secondary	2d Vortex	$500 \leq Gr < 515$	VF (Vortex flow)	VF
Tertiary	Oscillatory	$515 \leq Gr < 593$, $640 < Gr < 649$ $661 \leq Gr < 740$	OSV flow (subharmonic)	
Tertiary	Oscillatory and axially drifting	$543 \leq Gr \leq 750$		OSV flow (superharmonic)
Quaternary	Oscillatory and axially drifting	$593 \leq Gr \leq 640$, $649 \leq Gr \leq 660$ and $740 \leq Gr < 770$	OSAD flow (Oscillatory Subharmonic u-drift flow)	—
Quinary	Oscillatory axially and azimuthally drifting	$770 \leq Gr < 810$	OSAZD flow (Oscillatory Subharmonic u-drift and v-drift flow)	—

Table 2: Range of Grashof number values for the rectangular tube and for specific choices of the wavenumber values $(\alpha, \beta) = (1.34, 0.7)$ for the subharmonic case and $(\alpha, \beta) = (1.34, 1.34)$ for the superharmonic route.

the superharmonic OPV state. Both states were identified via direct forward marching numerical simulations. A higher truncation level with $(L, M, N) = (23, 14, 14)$ was also used for the verification of this state to ensure that the state was captured accurately.

In Figure 5 the Oscillatory Quinary axially and azimuthally drifting Subharmonic State (OSAZD) of the laterally heated rectangular tube. The results of the present analysis with $(L, M, N) = (21, 10, 10)$ are given, for $Pr = 0, Gr = 770$ and $(\alpha, \beta) = (1.34, 0.7)$. The state bifurcates from the quaternary state with $(\alpha, \beta) = (1.34, 0.7)$ and has the same wavenumbers. The higher truncation level $(L, M, N) = (23, 14, 14)$ was also applied to ensure that the state was captured accurately. These quinary states were identified with DNS only.

In Figure 6 we compare two tertiary states in the subharmonic SBA to turbulence for the laterally heated rectangular tube. The results of our analysis with $(L, M, N) = (21, 10, 10)$ are given, for $Pr = 0, Gr = 640(a), 740(b)$. For both states $(\alpha, \beta) = (1.34, 0.7)$. The states were captured via DNS. A higher truncation level with $(L, M, N) = (23, 14, 14)$ was also applied for the identification of the states to ensure that the states were captured accurately. In Figure 6 we see the loss of the flat surface boundaries between hot and cold regions and the emergence of wavy surfaces. This re-alignment of the vortices maximizes momentum and mass transfer.

In Figure 7 the quaternary OSAD (drifting in the azimuthal direction) subharmonic state and the tertiary Oscillatory Superharmonic axially drifting (OPV) flow of the laterally heated vertical rectangular tube of Figure 1 are presented. The results of the present analysis with $(L, M, N) = (21, 10, 10)$ are given, for $Pr = 0$. Here left column (part (a)) for the quaternary OSAD and right column (part b) the tertiary OPV and for $Gr = 640$. The states are depicted by their corresponding planar countour plots and $(\alpha, \beta) = (1.34, 1.34)$ for OPV and $(\alpha, \beta) = (1.34, 0.7)$ for OSAD. Both states were captured via DNS. As is evident from this figure and following our analysis that we present for the superharmonic route in Table 2 we conclude that the tertiary superharmonic state OPV is a subset of the subharmonic manifold of solutions. The suprharmonic route offers no further bifurcations and the superharmonic OPV eventually becomes unstable for further increases of the Grashof number values beyond $Gr = 780$.

In Figure 8 we offer a comparison between the subharmonic tertiary OBV (a) and the quinary azimuthally and axially drifting state (OSAZD) of the laterally heated rectangular tube. The results of the present analysis with $(L, M, N) = (23, 14, 14)$ are given, for $Pr = 0, Gr = 710$ (a) and $Pr = 0, Gr = 770$ (b). Here $(\alpha, \beta) = (1.34, 0.7)$ for both states. The quinary state bifurcates from the quaternary state at $Gr = 770$. This state cannot be identified by Newton Raphson method as it is also not a steady localised solution.

5. Concluding remarks

In the present study we employed a variety of proprietary code that is capable of capturing solutions that describe steady states, drifting waves with a uniform velocity or combinations of these type of solutions. For these types of solutions fixed points in the Poincaré map are taken to be the 'stable' periodic states as an initial guess, which are also available in the DNS and are used to calculate the return map on the Poincaré section, where one of the expansion coefficients, $a_{\ell mn}, b_{\ell mn}, c_\ell, d_\ell$, is constant. In order to evaluate the Jacobian matrix numerically the other expansion coefficients are changed slightly one by one. Their return maps are also created by the DNS and are used to approximate the Jacobian matrix by a linear finite-difference scheme. Additionally the Newton-Raphson iteration is employed in these cases for consistency and cross-checking. The existence of the periodic solution is explored even in a region in the parameter space where it is unstable in order to fully understand its characteristics and its eventual loss of stability.

The amplitude of each nonlinear state that emerges from disturbances imposed on the laminar state grows gradually as the control parameter increases. The newly bifurcated nonlinear states emerge continuously and are initially stable to three

dimensional perturbations. Since the system transitions in our analysis smoothly changes from an unstable nonlinear state to the sequel initially stable nonlinear state as our control parameter Gr crosses a critical value, all bifurcations that we encountered were supercritical. In the present paper we have investigated the nonlinear development of the perturbations of the various states in the SBA and in the harmonic case using initially various numerical schemes. It transpired though that a variant of a direct numerical simulation, as described in section 4, was necessary for the higher order states as a Newton-Raphson iterative scheme could only capture the two dimensional VF. For all other states we employed the DNS route.

Our analysis for specific values of (α, β) has shown that there are two main routes for the transition o turbulence in a rectangular tube. The most transient route is the subharmonic one with the superharmonic case being a subset of the subharmonic one. A comparison of Figure 2 and Figure 3 shows that the tertiary states are characterised by flat boundaries between the hot and cold regions, while the quaternary states by wavy boundaries in the (x, y) planes. This means that the symmetry planes $x =$ constant is lost. In fact, there are two different solutions of the quaternary states. In addition the downward traveling solution exhibited in Figure 3 with mirror motion corresponding to a solution traveling upward which can be obtained by changing the sign of x and z in the representation of the solutions via eqs.(15-16). Which of the two solutions is realised in an actual experiment will depend, of course, on the application of the initial disturbance. The loss of symmetry with respect to the plane $z = 0$ and the emergence of he wavy boundaries for the higher order states can be attributed to the boundary conditions, see similar explanation for the Wavy Twist solution in [22] in relation to the experiments of [23].

In Figure 9 we depict the transition to turbulence for the quinary oscillatory subharmonic state (left) and the oscillatory tertiary superharmonic state (right). Both states are drifting in both axial and azimuthal directions of the laterally heated rectangular tube. The results of the present analysis are given, for $Pr = 0, Gr = 1000$ for both cases are presented in the Figure. A total of 2×10^{10} time steps were required to produce the figures depicted here. Here $\alpha, \beta = 1.34, 0.7$ for the subharmonic state on the left and $(\alpha, \beta) = (1.34, 1.34)$ for the superharmonic state on the right. These states cannot be identified by Newton Raphson method as they are not a steady localised or uniformly moving solutions. The supeharmonic state retains its quasi-periodicity up tp $Gr = 2000$. Higher truncation levels were required for the identification of the sequence of transient states presented in Figure 9.

An interesting and unusual property of the quaternary subharmonic solutions is their return to the oscillatory tertiary three-dimensional solution at a higher value of the control parameter Gr, i.e. in between the regions mentioned in Table 2. This may not be a physically realistic scenario since we did not examine other bifurcation points on the branch of the tertiary oscillatory solutions as well as on the branches of the oscillatory drifting solutions, restricting our investigation to equivalent cases of the Floquet ansatz of eqs.(28-29) to $d = \alpha/2, b = \beta$. We cannot exclude therefore the existence of simpler or more complicated structures with a different choice of (d, b) values. It appears however that the imposition of the constant flux condition restricts the bifurcation path of the quaternary OSAD via re-aligning of the symmetries of the states until Gr becomes sufficiently high. Most of our calculations produced higher order states that have mean flow components in the axial and/or azimuthal directions.

Finally we note that all bifurcations in our study were supercritical and that the constant flux condition that we imposed makes the calculations realistic and close to the results of possible future laboratory experiments for direct comparisons with simulations. The case for $Pr \neq 0$ is currently under investigation.

6. Acknowledgments

This work was supported by a Horizon 2020 RISE award (Grant no. 824022) from the European Union. The large scale computations were performed using the High Performance Computing facilities Nandi of Aston University . This work was also supported by the Japanese Society for the Promotion of Science (JSPS) KAKENHI Grant Number JP23K03334.

Declaration of Interest Statement

All authors have no conflicts of interest.

References

[1] D. I. Boyarintsev, Heat transfer through liquid and gaseous layers, Moscow Power Engineering Institute, Academy of Sciences of the USSR Candidate's Dissertation (1941).

[2] Y. Chen, A. J. Pearlstein, Stability of free-convection flows of variable viscosity fluids in vertical and inclined slots, J . Fluid Mech. 198 (1989) 513–541.

[3] D. I. Boyarintsev, Heat transfer through liquid and gaseous layers, J. Tech. Phys 20 (1950) 1084.

[4] G. Gershuni, On the stability of plane convective motion of a fluid., Zh. Techn. Fiz. 23 (1953) 1838.

[5] G. Gershuni, On the problem of stability of plane convective motion of liquids., Zh. Techn. Fiz. 25 (1955) 351.

[6] N. Rudakov, Spectrum of perturbations and stability of convective motion between vertical plane, J. Appl. Math. and Mech. 31 (1967) 376–383.

[7] C. M. Vest, V. S.Arpaci, Stability of natural convection in a vertical slot, J . Fluid Mech. 36 (1969) 107–117.

[8] R. V. Birikh, G. Z. Gershuni, E. M. Zhukhovitskii, R. N. Rudakov, Stability of the steady convective motion of a fluid with a longitudinal temperature gradient, Phys. Met. Metallogr. 33 (1969) 958.

[9] S. A. Korpela, D.Gözüm, C.B.Baxi, On the stability of the conduction regime of natural convection in a vertical slot, Int. J. Heat and Mass Trans. 16 (1973) 1683–1690.

[10] R. F. Bergholz, Instability of steady natural convection in a vertical fluid layer, J .Fluid Mech. 84 (1978).

[11] K. Fujimura, J. Mizushima, Nonlinear equilibrium solutions for travelling waves in a free convection between vertical parallel plates, Eur. J. Mech. B/Fluids, [Suppl.2] 10 (1991) 25–30.

[12] M. Kropp, F. H. Busse, Multiple bifurcation of free convection between vertical parallel plates, International Series of Numerical Mathematics, ed. R. Seydel, F. W. Schneider, T. Küpper, and H. Troger (Birkhäuser, Basel) 97 (1991) 217–223.

[13] M. Nagata, F.H.Busse, The stability of natural convection in a vertical fluid layer, J. Fluid Mech. 169 (1983) 1–26.

[14] H. Squire, On the stability for three-dimensional disturbances of viscous fluid flow between parallel walls, Proc. R. Soc. Lond. Ser. A Math. Phys. Eng. Sci. 142 (1933) 621–628.

[15] W. Eckhaus, Studies in non-linear stability theory, Springer ISBN 9783642883170 (1965) 118.

[16] R. Meyer-Spasche, H. B. Keller, Some bifurcation diagrams for taylor vortex flows, Phys. Fluids 28 (1985) 1248–1252.

[17] H.-G. Paap, H. Riecke, Wave-number restriction and mode interaction in taylor vortex flow: Appearance of a short-wavelength instability, Phys. Rev. A 41 (1990) 1943–1951.

[18] K. Fujimura, J. Mizushima, Nonlinear interaction of disturbances in free convection between vertical parallel plates, in Nonlinear Wave Interactions in Fluids, ed. R. W. Miksad, T. R. Akylas, and T. Herbert, (ASME, New York) 41 (1990) 123–130.

[19] J. Mizushima, Mechanism of mode selection in Rayleigh-Bénard convection with free-rigid boundaries, Fluid Dyn. Res. 11 (1993) 297–311.

[20] T. Itano, S. C. Generalis, Hairpin vortex solution in planar couette flow: A tapestry of knotted vortices, Phys. Rev. Lett. 102 (2009) 114501.

[21] S. C. Generalis, T. Itano, Characterization of the hairpin vortex solution in plane couette flow, Phys. Rev. E 82 (2010) 066308.

[22] T.Akinaga, S.C.Generalis, F.H.Busse, Tertiary and quaternary states in the taylor-couette system, Chaos Sol. & Fr. 109 (2018) 107–117.

[23] J. J. Hegseth, G. W. Baxter, C. D. Andereck, Bifurcations from Taylor vortices between corotating concentric cylinders., Phys. Rev. E 53 (1996) 507–521.

[24] L. Rayleigh, On the stability or instability of certain fluid motions, Proc. Lond. Maths. Soc. 11 (1880) 57–70.

[25] T. Akinaga, T. Itano, S. Generalis, Convection induced by instabilities in the presence of a transverse seepage, Chaos Sol. and Frac. 91 (2016) 533–543.

[26] E. Weisshaar, F. H. Busse, M. Nagata, Twist vortices and their instabilities in the Taylor-Couette system., J. Fluid Mech. 226 (1991) 549–564.